Sintering behavior of a six-oxide silicate bioactive glass for scaffold manufacturing

applied sciences

MDPI

Article

Sintering Behavior of a Six-Oxide Silicate Bioactive Glass for Scaffold Manufacturing

Elisa Fiume [1,2,*], Gianpaolo Serino [1], Cristina Bignardi [1], Enrica Verné [2] and Francesco Baino [2,*]

[1] Department of Mechanical and Aerospace Engineering (DIMEAS), Politecnico di Torino, 10129 Torino, Italy; gianpaolo.serino@polito.it (G.S.); cristina.bignardi@polito.it (C.B.)

[2] Institute of Materials Physics and Engineering, Department of Applied Science and Technology (DISAT), Politecnico di Torino, 10129 Torino, Italy; enrica.verne@polito.it

* Correspondence: elisa.fiume@polito.it (E.F.); francesco.baino@polito.it (F.B)

Received: 31 October 2020; Accepted: 20 November 2020; Published: 22 November 2020

Abstract: The intrinsic brittleness of bioactive glasses (BGs) is one of the main barriers to the widespread use of three-dimensional porous BG-derived bone grafts (scaffolds) in clinical practice. Among all the available strategies for improving the mechanical properties of BG-based scaffolds, strut densification upon sintering treatments at high temperatures represents a relatively easy approach, but its implementation might lead to undesired and poorly predictable decrease in porosity, mass transport properties and bioactivity resulting from densification and devitrification phenomena occurring in the material upon heating. The aim of the present work was to investigate the sinter-crystallization of a highly bioactive SiO_2-P_2O_5-CaO–MgO–Na_2O–K_2O glass (47.5B composition) in reference to its suitability for the fabrication of bonelike foams. The thermal behavior of 47.5B glass particles was investigated upon sintering at different temperatures in the range of 600–850 °C by means of combined thermal analyses (differential thermal analysis (DTA) and hot-stage microscopy (HSM)). Then, XRD measurements were carried out to identify crystalline phases developed upon sintering. Finally, porous scaffolds were produced by a foam replica method in order to evaluate the effect of the sintering temperature on the mechanical properties under compression loading conditions. Assessing a relationship between mechanical properties and sintering temperature, or in other words between scaffold performance and fabrication process, is a key step towards the rationale design of optimized scaffolds for tissue repair.

Keywords: bioactive glass; sintering; scaffold; bone tissue engineering; mechanical properties; bioactivity

1. Introduction

Among all the available biomaterials optimized up to now for bone regenerative strategies, bioactive glasses (BGs) indeed deserve special attention [1]. The reason for such a keen scientific interest, which is still arising even fifty years after the invention of the first BG composition (Hench's 45S5) [2], lies on their high reactivity in physiological environment resulting in tissue-bonding capabilities. It is well known that the precipitation of hydroxyapatite crystals on BG surface [3,4] allows creating a stable bonding interface between the material and the native tissue and promotes osteointegration processes [5]. In this way, the glass gradually dissolves over time, concurrently with the formation of new, healthy tissue [6].

In clinics, BGs have been widely employed in form of fine powders and particulates, especially in dentistry and orthopedics, where their use is firmly established since many years due to their ability to promote bone remineralization [7], as well as their enormous potential as bioactive coatings on inert metal implants [8–10].

Recently, the desire to optimize bone tissue engineering strategies for supporting bone regeneration in medium to critically sized defects has shifted the attention toward the optimization of three-dimensional (3D) porous scaffolds able to provide mechanical support and stimulate osteogenetic pathways in all those cases in which the physiological self-healing capability of bone appears to be seriously compromised, such as in surgical tumors resection, traumas and congenital diseases [11,12].

In this regard, the exceptional behavior of BGs in contact with body fluids, as well as the possibility to perform high-temperature treatment to obtain highly densified structures by particles sintering, makes indisputable their enormous potential as basic materials for the production of porous scaffolds for bone tissue engineering application [13].

Moreover, the extreme versatility of BGs allows them to be successfully processed in the form of porous architectures by a wide series of manufacturing techniques, including replication of porous templates [14–17], foaming methods [18–20] and, more recently, free-form fabrication strategies, also known under the name of additive manufacturing (AM) technologies [21,22].

However, despite remarkable technological advances in recent years, the intrinsic brittleness and the low resistance to crack propagation, typical of glass and ceramic materials, still limit the use of BG-based scaffolds in clinical practice, due to the objective difficulty in guaranteeing mechanically reliable structures suitable for a safe usage, especially in load-bearing applications [23].

Apart from the possibility to coat or infiltrate the scaffold with a degradable polymer, which draws inspiration from the natural toughening mechanism of bone [24,25], one of the most common and easiest strategies to improve the mechanical performances of BG-based scaffolds relies on the material's densification phenomena upon sintering processes [26,27].

As an example, Jones and coworkers found that increasing the sintering temperature of sol-gel foamed binary scaffolds from 600 to 800 °C led to an improvement in compressive strength from 0.34 to 2.26 MPa, as a consequence of the thickening of the pore walls and a decrease in textural properties [27].

Most BGs exhibit the tendency to partially crystallize during sintering, thus transforming into glass-ceramic materials [28]. The most famous example is 45S5 Bioglass®, for which the Q^n (Si) distribution (n = number of bridging oxygens) results in a structure dominated by chains of Q^2 metasilicates that are occasionally cross-linked through Q^3 units, whereas the Q^1 species terminate the chains distribution. The final result is a highly disrupted silicate network with high reactivity in physiological environment, as well as low glass transition temperature and enhanced devitrification tendency upon heating due to the low chemical stability of the network [29].

When a glass devitrifies, the crystalline phases which nucleate and grow within the amorphous matrix not only improve the strength of the material, but also make it chemically more stable [29–31]. In this regard, one of the major concerns related to the sinter-crystallization of BGs is in fact the subsequent decrease in bioactive potential, as the ion-release phenomena involved in the mechanism of bioactivity are mainly related to the amorphous phase. As a result, the optimal sintering window for BG processing is conventionally defined between the glass transition temperature and the crystallization onset of the material. Within this range, the temperature is not high enough to induce devitrification of the system but sufficient to allow the formation of sintering necks between adjacent glass particles through viscous flow and diffusive mechanisms, thus ideally preserving the glass bioactivity.

However, the nucleation of crystalline phases is not the only factor affecting the reactivity of BGs and an optimal design of glass composition could be effective in conferring high bioactive potential to the material despite devitrification phenomena. Since 2009, the multicomponent 47.5B BG, with composition 47.5SiO_2-2.5P_2O_5-20CaO–10MgO–10Na_2O–10K_2O (mol. %), has been highly appreciated for its wide workability window, thus allowing the production of highly densified structures while preserving its amorphous nature and excellent apatite-forming ability [32]. In addition, more recent studies proved that its bioactive potential can be preserved also at higher sintering temperatures, despite the development of crystalline phases [16,20].

In a recent previous study, the effects of the sintering temperature on the overall microstructural properties of 47.5B-based scaffolds produced by the foam replication technique were determined

as a function of the sintering temperature by combining mathematical modeling and experimental measurements of intrinsic permeability supported by tomographic characterization [33].

With the present study, the authors aim at completing the characterization of 47.5B-based scaffolds. In particular, the behavior of 47.5B BG upon thermal treatment was investigated in detail by means of isothermal differential thermal analysis (DTA) and hot-stage microscopy (HSM) measurements. The sintering process was simulated at six different temperatures, defined between 600 °C and 850 °C and corresponding respectively to the beginning of viscous flow phenomena and the end of crystallization of the glass, as previously reported [34]. Development of crystalline phases was assessed by XRD analyses and scaffolds produced by foam replica method underwent compressive tests in order to investigate the effect of the different thermal treatment on scaffold mechanical strength.

2. Materials and Methods

2.1. Glass Production

47.5B BG, with composition 47.5 SiO_2–2.5 P_2O_5–20 CaO–20 MgO–10 Na_2O–10 K_2O (mol. %), was produced by melt-quenching route as previously described [16,20,21,32]. Silica (SiO_2), calcium carbonate ($CaCO_3$), calcium phosphate ($Ca_3(PO_4)_2$), magnesium carbonate hydroxide pentahydrate ($(MgCO_3)_4Mg(OH)_2{\cdot}5H_2O$), sodium carbonate ($Na_2CO_3$) and potassium carbonate (K_2CO_3) were used as precursors of glass oxides. Briefly, rough reagents were mixed in proper amounts on rotating rollers overnight. Then, the powders were hand-pressed into a platinum crucible, covered with a platinum cap and heated up to 1000 °C (heating rate: 12 °C/min, dwelling time: 10 min) into a high-temperature furnace (Nabertherm 1800 GmbH, Lilienthal, Germany) in order to allow decomposition of carbonates. Then, the cap was removed and the temperature was raised up to 1500 °C with a heating rate of 15 °C/min and maintained constant for 1 h to obtain a homogeneous melt. Afterwards, the melt was poured into distilled water to obtain a glass frit, which was then crushed by ball milling and sieved to obtain a final grain size below 32 µm.

2.2. Scaffold Manufacturing

47.5B-based scaffolds were produced by foam replica method as previously reported elsewhere [33]. Briefly, polyurethane (PU) sponges (45 ppi) were shaped into cylinders with diameter of 14 mm and height of 10 mm by means of a cutting die. In order to prepare the glass slurry, particles of polyvinyl alcohol were dissolved into water under continuous magnetic stirring (200 rpm, 50 °C); then, the solution was cooled at room temperature and glass powders were added in proper amounts (PVA:H_2O:47.5B = 6:64:30, wt. %). The suspension was mixed at room temperature for about 5 min, maintaining a stirring rate of 200 rpm. Each cylindric sponge was dipped into the slurry three times. After each immersion, the sponge was placed onto a metallic grid and the excess slurry was squeezed out from the pores by applying an instantaneous compression load, as described in [33]. The green bodies were dried overnight at room temperature and heat treated at different sintering temperatures in order to investigate the effect of the thermal treatment on scaffolds mechanical properties. Six different sintering temperatures were identified in the range 600–850 °C, spaced of 50 °C, selected on the basis of non-isothermal Differential Thermal Analysis results, (previously reported in [34]). The thermal treatment was performed in an electrical furnace (Nabertherm Muffle Furnace 1100°C L9/11/SKM/P330, Lilienthal, Germany) using a heating rate of 5 °C/min, three-hour dwell at each sintering temperature (T_s = 600, 650, 700, 750, 800 and 850 °C) and a cooling rate of 10 °C/min up to 25 °C.

2.3. Thermal Analyses: DTA and HSM

The sintering behavior of 47.5B BG was investigated by differential thermal analysis (DTA) and hot-stage microscopy (HSM) by using a DTA 404 PC instrument (Netzsch, Selb, Germany) and HSM EMI III (Hesse Instruments, Osterode am Harz, Germany), respectively; in order to simulate the same

sintering treatment described for scaffold manufacturing, the thermal cycle was performed by setting a multistage program, composed as follows:

- Step 1: from 20 to 400 °C, heating rate 60 °C/min;
- Step 2: from 400 to T_s, heating rate 5°C/min;
- Step 3: 3 h-dwell, T_s.

For DTA measurements, 100 mg of 47.5B glass powders were introduced in Pt-Rh crucibles provided by the manufacturer and high-purity (99%) Al_2O_3 was used in the same amount as a reference material.

For HSM measurements, cylindrical samples of 47.5B pressed powders with a diameter of 3 mm and height of 3 mm were positioned onto a high purity alumina plate inside the furnace chamber; black and white images showing the silhouettes of the samples were acquired during the whole duration of the test and analyzed by means of a dedicated image analysis software (EMI III- Software für das Erhitzungsmikroskop, Hesse Instruments, Osterode am Harz, Germany). Sample shrinkage ΔH was quantified in terms of normalized height (h/h_0) as a function of both time and temperature, where h_0 was the height of cylindrical sample at the beginning of the test (3 mm) and h was the actual height of the sample measured during the analysis.

2.4. X-ray Diffraction

For XRD surface analysis, six glass tablets of 12 mm diameter and 2 mm height were prepared by pressing 47.5B glass powders using a manual hydraulic press (P400ir Cagimbra, Italy; 1.4 MPa, 15 s) and each tablet was sintered at a different temperature, according to the six thermal treatments described above. Before the analysis, the surface of the sintered tablets was polished using 320–4000 grit SiC papers at 500 rpm. X-Ray Diffraction analysis (XRD; 2θ within 10–70°) was performed to identify the crystalline phases by using a X'Pert Pro PW3040/60 diffractometer with a Bragg-Brentano camera geometry and Cu Kα incident radiation λ = 0.15405 nm (PANalytical, Eindhoven, The Netherlands; parameters: operating voltage 40 kV, filament current 30 mA, step size 0.02°, counting time per step 1 s). Identification of crystalline phases was carried out by using X'Pert HighScore software 2.2b (PANalytical, Eindhoven, The Netherlands) equipped with the PCPDFWIN database (http://pcpdfwin.updatestar.com).

2.5. SEM Morphological Characterization

Particles' densification level upon sintering and scaffold morphology at different sintering temperatures was investigated by Scanning Electron Microscopy (SEM) analyses (FE-SEM MERLIN™, Carl Zeiss, Vienna, Austria) using an accelerating voltage in the range 5–15 kV. Before the analysis, a conductive layer of chromium was sputtered on the surface of the samples (7 nm).

2.6. Mechanical Tests

The compressive strength of foam-replicated scaffolds was assessed in triplicate for each sintering group. Prior to performing mechanical tests, the surfaces of all the samples were rectified by gentle polishing procedure using grit 800–1000 SiC papers.

All the scaffolds were characterized in terms of diameter D, height H, cross-sectional area A, and mass m. The apparent density of the scaffolds ρ_a was calculated as mass-to-volume ratio, while the total porosity ε_0 was derived according to Equation (1), as previously reported by Karageorgiou and Kaplan [35]:

$$\varepsilon_0 = 1 - \frac{\rho_a}{\rho_{glass}} \quad (1)$$

where ρ_{glass} = 2.67 g/cm^3 is the density of the bulk material, determined in a previous work [36].

Results were expressed as mean value ± standard deviation calculated on three scaffolds for each sintering group (Table 1).

Table 1. Geometrical characterization of foam-replicated scaffolds used for mechanical testing. Values are expressed as mean value ± standard deviation, calculated on three samples for each sintering group.

Sintering Temperature T/°C	600	650	700	750	800	850
Diameter D/mm	8.61 ± 0.27	8.01 ± 0.63	10.62 ± 0.41	8.85 ± 0.14	9.68 ± 0.12	8.70 ± 0.47
Height H/mm	7.04 ± 0.14	6.11 ± 0.11	6.24 ±0.43	6.00 ± 0.58	7.51 ± 0.39	6.65 ± 0.32
Cross sectional area A/mm^2	58.31 ± 3.70	51.07 ± 7.73	88.84 ± 6.86	61.77 ± 2.02	73.67 ± 1.80	59.68 ± 6.30
Mass m/g	0.250 ± 0.02	0.243 ± 0.01	0.285 ± 0.02	0.325 ± 0.03	0.249 ± 0.03	0.259 ± 0.02

Destructive crushing tests were performed by using an MTS machine (QTestTM/10). A cell load of 10 kN and a cross-head speed of 0.5 mm/min were used for all the samples. The maximum compressive strength σ_{max} was calculated as the ratio between the maximum load registered during the test and the resistant cross-sectional area. The results were expressed as mean ± standard deviation.

3. Results and Discussion

BGs are commonly recognized to be promising materials for the production of 3D structures for bone tissue engineering applications [37]. However, the use of BG-based scaffolds is still limited in clinical practice due to the tendency of these materials to crystallize upon heating treatments, with undesired and sometimes unpredictable effects on their macroporous structure and bioactive properties in contact with body fluids.

One of the main concerns related to the crystallization of BGs upon sintering is in fact the partial loss in the bioactive potential, as the ion-exchange mechanisms involved in the process of deposition of the hydroxyapatite reaction layer are mainly attributed to the amorphous glassy matrix, while crystalline species are usually characterized by lower reaction kinetics in aqueous environment.

Despite this, producing dense glass-ceramic scaffolds is sometimes necessary to achieve better mechanical performances and obtain structures able to support the physiological healing process of bone tissue while maintaining mechanical integrity over the whole duration of the therapeutic treatment.

As a result, when designing a BG-based scaffold for bone regeneration, achieving the right balance between mechanical, morphological and bioactive properties has to be considered as a primary need.

The silicate 47.5B BG, based on the six oxides system SiO_2-P_2O_5-CaO-MgO-Na_2O-K_2O, was greatly appreciated in the past for its wide workability window, which makes it possible to obtain highly densified structures upon sintering in a wide range of temperatures without inhibiting the reactivity of the system in contact with body fluids.

In a previous study, it was demonstrated that the activation energy for viscous flow in 47.5B glass, assessed by the Kissinger and Matusita–Sakka equations, is lower than that required for crystallization, thus proving the potentiality of this material to achieve significant densification levels before the beginning of devitrification processes upon thermal treatments above T_g [34].

In addition, other studies showed that 47.5B composition is able to retain its exceptional apatite-forming ability even at temperatures much higher than the crystallization onset of the system [20]. This can be partly explained by the fact that 47.5B composition, designed by Verné and coworkers in 2009 [32], exhibits a high Ca/P ratio (just like Hench's 45S5 Bioglass® [4]), which ensures good bioactivity in physiological environment even in spite of devitrification phenomena upon thermal treatments.

As a result, in recent years, 47.5B glass has been extensively employed in the production of highly densified and bioactive porous scaffolds for bone tissue engineering applications by different manufacturing processes [16,20,21,36,38].

In the present work, thermal analyses were performed to simulate the pressure-less sintering process of 47.5B BG particles at different temperatures, in order to investigate the evolution of the glassy system upon heating; moreover, the effect of sintering temperature on glass devitrification and scaffolds mechanical properties was investigated by XRD and compression mechanical test.

Figure 1 shows the graphical output of DTA measurements, while Table 2 summarizes the characteristic temperatures of the six systems analyzed.

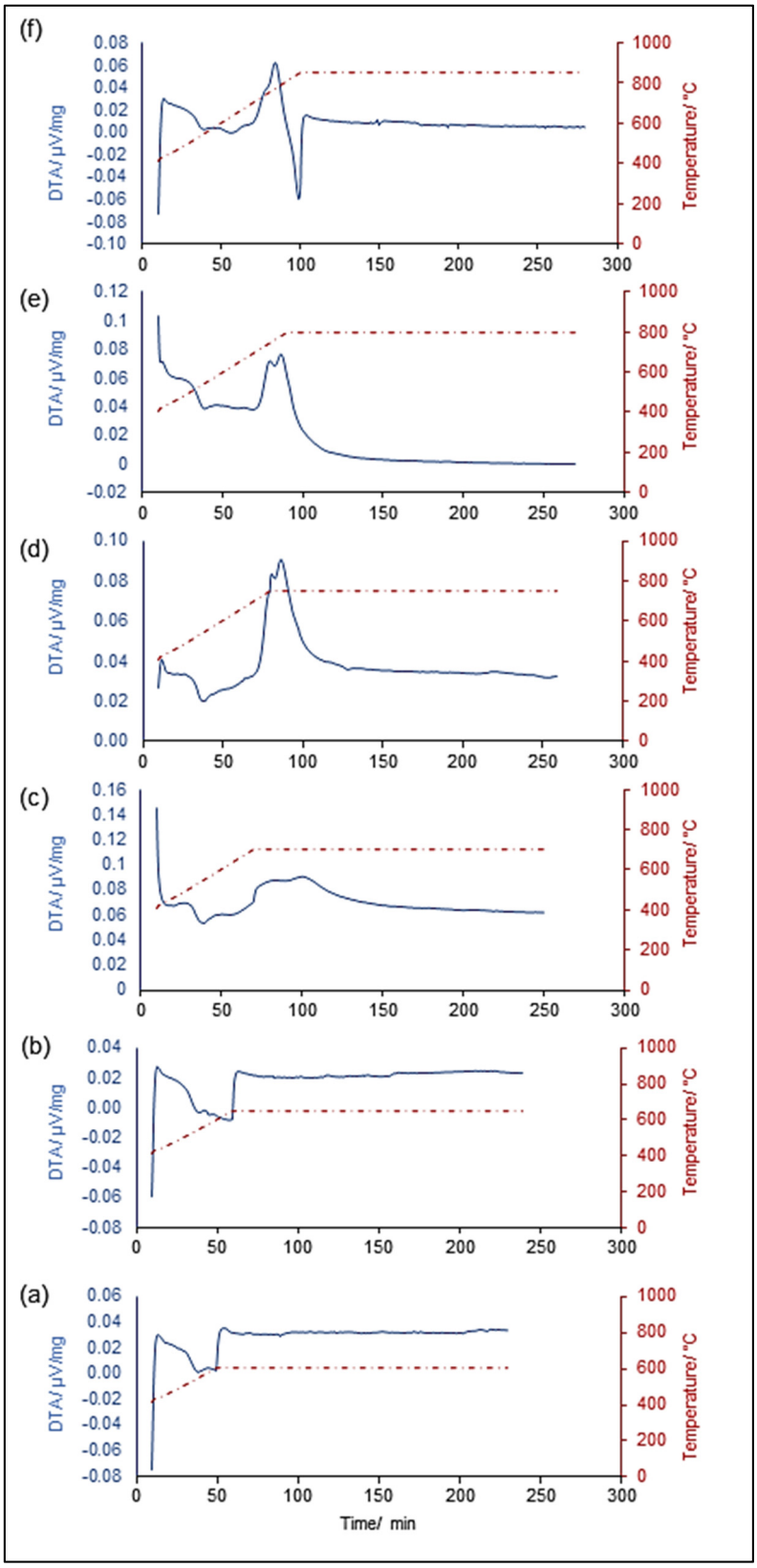

Figure 1. Differential thermal analysis (DTA) simulating the sintering treatment at different temperatures: 600 °C (**a**), 650 °C (**b**), 700 °C (**c**), 750 °C (**d**), 800 °C (**e**) and 850 °C (**f**).

Table 2. Characteristic temperatures of 47.5B bioactive glass sintered at different temperatures assessed by DTA measurements under isothermal conditions.

Sintering Temperature T/°C	Glass Transition T_g/°C	Crystallization Onset T_c/°C	Crystallization Peak T_p/°C	Maximum Shrinkage ΔH/%
600	527	-	-	24
650	528	-	-	28
700	528	-	-	27
750	527	690	750	18
800	530	707	750, 783	21
850	531	697	772	29

For each curve reported in Figure 1, glass transition temperature T_g was defined within the range 527–531°C, in correspondence of the inflection point, while the crystallization onset T_x was identified at the onset point of the exothermic peaks (Figure 1d–f), between 690 and 707 °C, in good agreement with the temperature ranges previously reported in non-isothermal conditions [34].

Glass powders sintered below the crystallization onset (Figure 1a,b) did not undergo any crystallization and DTA curves referred to these systems were characterized by no exothermic peaks. A steplike increase was observed in correspondence of the beginning of the dwell stage, most likely attributed to the shift to isothermal conditions in the program settings. A similar trend, in fact, was also observed in Figure 1c and d but was completely hidden for the glasses heated up to 800 and 850 °C (Figure 1e,f), due to the overlap of the exothermic crystallization peaks.

A mild crystallization was observed for a sintering temperature of 700 °C, after about 30 min from the beginning of the dwelling stage (Figure 1c); compared to the previous DTA thermograms acquired at 600 °C and 650 °C, which presented a flat trend in stasis, this curve evolved in a broad hump, suggesting the beginning of devitrification phenomena. This hypothesis was strongly supported by the range of crystallization onset previously provided.

As expected, the "hump" observed for temperature close to the glass crystallization onset evolved into sharp exotermic peaks approaching higher sintering temperatures (Figure 1d–f).

As a first approximation, it seemed that the exotermic signals observed at 750 and 800 °C presented analogous features. Both of them, in fact, consisted of two different peaks, closely located. However, some additional considerations could be made if the position of these signals with respect to the temperature-time dashed curve is considered. In the system treated at 750 °C, the two exothermic peaks are both registered at the end of the heating ramp, at a constant temperature of 750 °C (Figure 1d). On the contrary, the peaks observed in Figure 1e developed upon heating at 750 and 783 °C, respectively, with a time delay of about 6 min. It is worth observing that the curve related to the glass sintered at 850 °C (Figure 1f) presented a single peak centered at 772 °C, ending in correspondence of the beginning of the 850 °C dwell, indicating that glass devitrification is already completed before the beginning of the dwelling stage.

In order to explain this, two different hypotheses can be proposed:

(i) the nucleation of a metastable crystalline phase at 750 °C, which gradually evolves to a second more stable crystalline system, resulting in a second exothermic signal at temperatures T ≥ 800 °C;

(ii) the nucleation of two different metastable phases at 750 °C and 780 °C, which evolve to a third crystalline system stable at temperatures ≥ 850 °C.

In this regard, XRD analyses performed on sintered 47.5B tablets confirmed the progressive nucleation of crystalline species with increasing sintering temperatures. XRD patterns related to the samples sintered at different temperature are depicted in Figure 2.

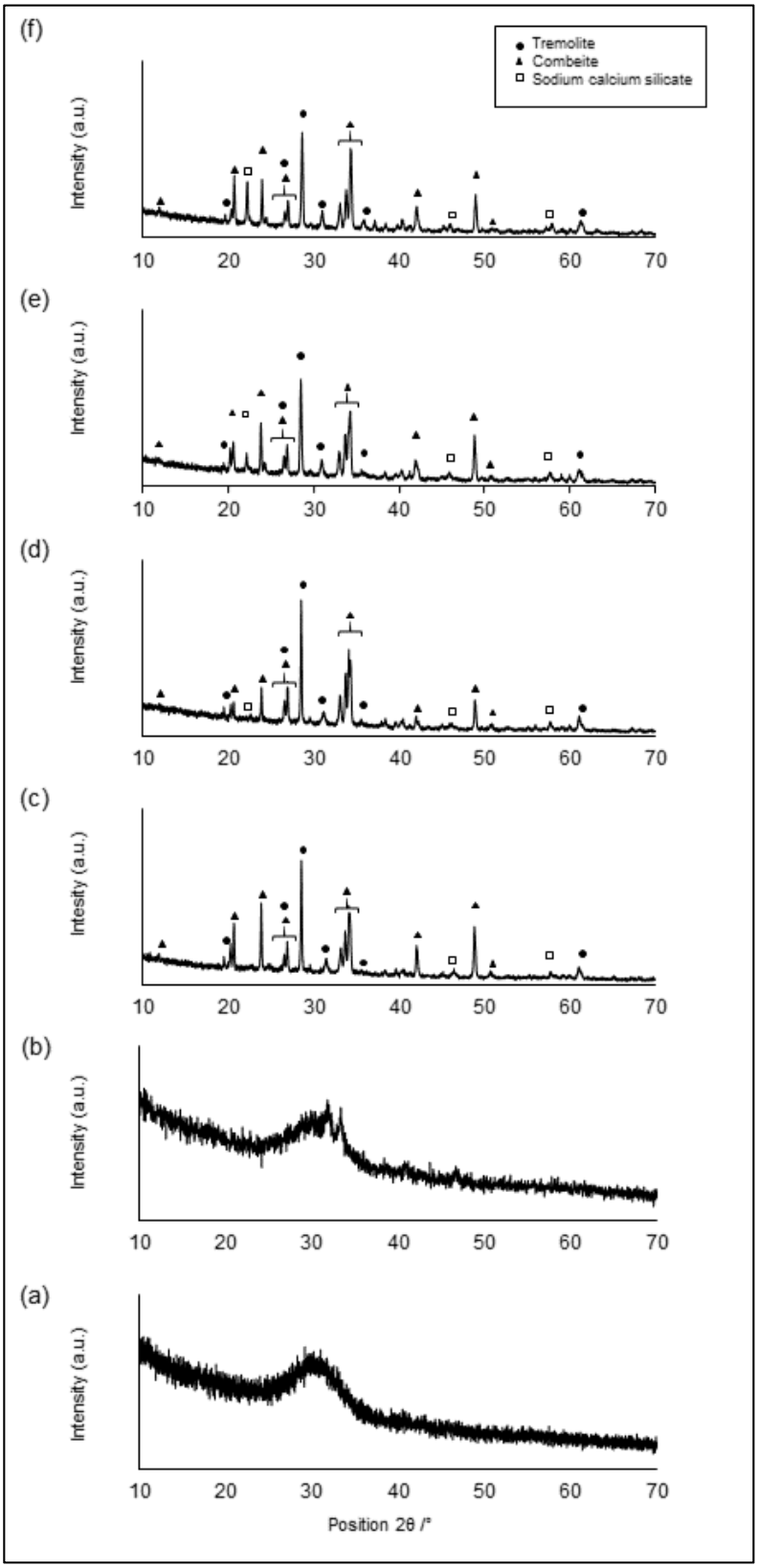

Figure 2. XRD patterns of 47.5B tablets sintered at different temperatures: 600 °C (**a**), 650 °C (**b**), 700 °C (**c**), 750 °C (**d**), 800 °C (**e**) and 850 °C (**f**).

As expected, specimens sintered below the crystallization onset, at 600 and 650 °C (Figure 2a,b), revealed no diffraction peaks and were characterized by an amorphous halo typical of silicate glasses

for 2θ values ranging between 25° and 35°, thus indicating that no microstructural changes occurred within the material as a result of these sintering treatments.

On the contrary, the patterns of samples treated at 700, 750, 800 and 850 °C presented multiple diffraction peaks, which are typical of glass-ceramic materials, as might be predicted from DTA thermograms. Crystalline phases detected above the crystallization onset are summarized in Table 3.

Table 3. Crystalline phases detected in 47.5B samples sintered at 700, 750, 800 and 850 °C.

Ref. Code	Compound Name	Chemical Formula	Crystal System
01-075-1686	Combeite	$Na_2Ca_2(Si_3O_9)$	Rombohedral
00-002-0455	Tremolite	$CaMg_3(SiO_4)_3$	Monoclinic
01-075-1332	Sodium-calcium silicate	$Na_{15.6}Ca_{3.84}(Si_{12}O_{36})$	Cubic

The analysis carried out on all the samples sintered at temperatures ≥ 700 °C revealed the presence of two main crystalline species, i.e., combeite ($Na_2Ca_2(Si_3O_9)$) and tremolite ($CaMg_3(SiO_4)_3$), together with other sodium-calcium silicates with different stoichiometry, to a lesser extent.

The formation of combeite ($Na_4Ca_4(Si_6O_{18})$) and akemanite ($Ca_2Mg(Si_2O_7)$, a calcium-magnesium silicate similar to tremolite, was already observed upon sintering treatment at high temperature (≥ 950 °C) in a silica-based experimental composition above, named CEL2, exhibiting the same oxides system of 47.5B [39].

Moreover, the formation of sodium-calcium silicate crystalline phases was also reported in our previous studies on the production of bread-templated and dolomite-foamed 47.5B-based scaffolds sintered at 750 °C and 800–850 °C, respectively; moreover, sodium-calcium silicate (combeite-type) phases were also reported to be the main crystalline species nucleating above 550 °C in 45S5 Bioglass®, which is commonly adopted as the positive control material among BGs in terms of bioactivity and citocompatibility standards [30,40].

Hot-stage microscopy (HSM) measurements under isothermal conditions were carried out in order to quantify the volumetric shrinkage of glass samples upon sintering at different temperatures. The sample shrinkage was quantified in terms of height percentage as a function of both time and temperature, as depicted in Figure 3; the values are summarized in Table 4.

As can be seen, it was not possible to observe a clear trend depending on the temperature increase since comparable values were registered for all the samples, regardless of the sintering conditions. Interestingly, the specimens sintered above 700 °C seemed to shrink less than all the others, with a progressive height reduction from 27 to 21%, with a minimum value of 18% registered at 750 °C in correspondence of the crystallization temperature of the glass. This could be likely attributed to microstructural adjustments resulting from the devitrification of the amorphous matrix, which becomes progressively stiffer due to the development of crystalline species, thus inhibiting densification phenomena. This is consistent with previous results reported by Huang et al. about the sinter-crystallization of 45S5 Bioglass®-derived glass-ceramic scaffolds [41].

A similar trend was also observed by Erasmus et al. [42] in borosilicate, borophosphate and phosphate glasses for bone regeneration. The study, indeed, reported that the density of the samples decreased as a result of the increase in sintering temperature due to the inhibition of viscous flow of the particles caused by crystallization phenomena at the material surface, thus reducing the densification ability of the material.

This was thought to have a clear effect on the mechanical performance of foam-replicated 47.5B-based scaffolds sintered at the same temperatures; the physical and structural parameters of such scaffolds are also collected in Table 4.

As can be seen, all the scaffolds examined in the present work exhibited compressive strength within the typical physiological ranges of human trabecular bone, defined between 0.1 and 16.0 MPa [37]. The total porosity of all samples is also within the typical range recommended for bone tissue engineering scaffolds (>0.50 [35]).

SEM morphological analyses revealed an improved densification of the 3D struts at high temperatures (Figure 4).

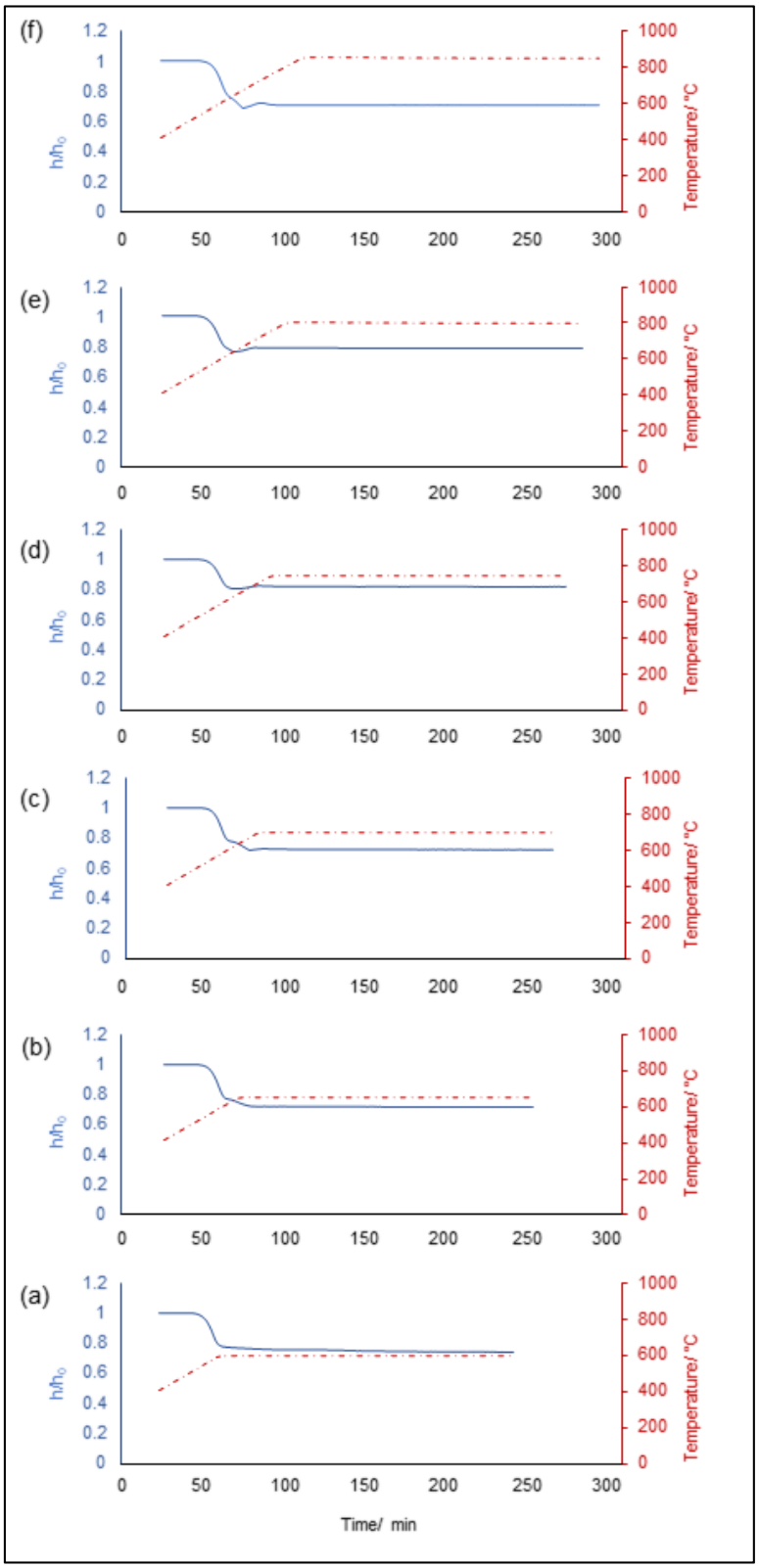

Figure 3. Hot-stage microscopy (HSM) analyses simulating the sintering treatment at different temperatures: 600 °C (**a**), 650 °C (**b**), 700 °C (**c**), 750 °C (**d**), 800 °C (**e**) and 850 °C (**f**).

Table 4. Physical and structural parameters of 47.5B-based bioactive glass and glass-ceramic scaffolds sintered at different temperatures within the 600–850 °C range.

Sintering Temperature T/°C	Apparent Density ρ_a /g/cm^3	Total Porosity ε_0	Maximum Shrinkage ΔH/%	Compressive Strength σ_{max}/MPa
600	0.62 ± 0.06	0.76 ± 0.2	24	0.49 ± 0.08
650	0.72 ± 0.07	0.72 ± 0.03	28	1.02 ± 0.44
700	0.41 ± 0.02	0.85 ± 0.01	27	1.47 ± 0.09
750	0.87 ± 0.03	0.67 ± 0.01	18	1.93 ± 0.06
800	0.47 ± 0.01	0.82 ± 0.01	21	1.61 ± 0.29
850	0.69 ± 0.03	0.73 ± 0.01	29	2.09 ± 1.02

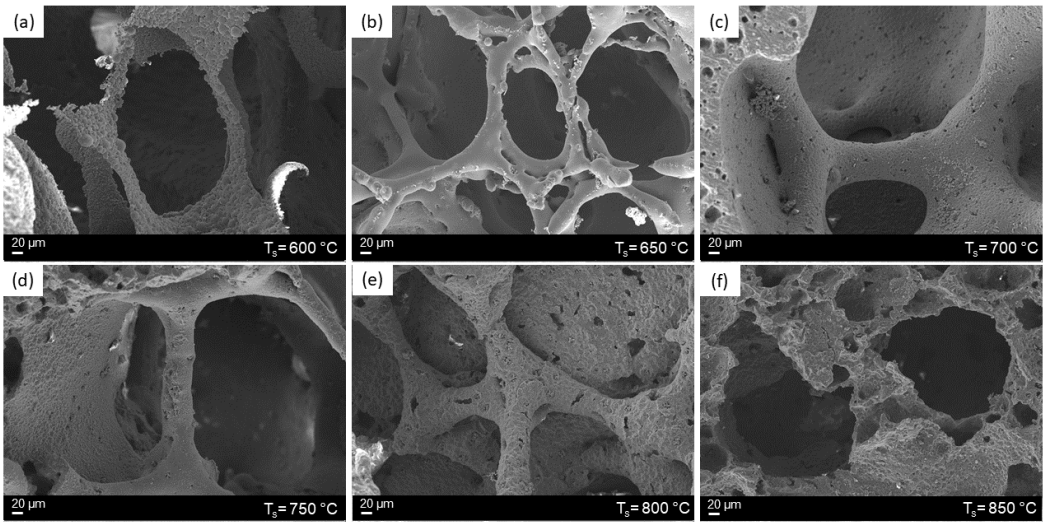

Figure 4. SEM images of 47.5B glass and glass-ceramic scaffolds sintered at different temperatures: 600 °C (**a**), 650 °C (**b**), 700 °C (**c**), 750 °C (**d**), 800 °C (**e**) and 850 °C (**f**).

In particular, while in Figure 4a, corresponding to the scaffold sintered at 600°C, adjacent glass particles are clearly delimited by visible borders, by increasing the sintering temperature, contact points between adjacent particles increased in number and sintering necks became gradually thicker, reducing progressively the interstitial voids (Figure 4b–d). As a result, the surface of scaffolds sintered between 650 and 750 °C appeared almost smooth and continuous, while the roughness observed in samples treated at 800 and 850 °C (Figure 4a,e,f) was related to the growing of crystalline phases on the scaffold's surface, as a result of the devitrification process of the glass.

As expected, an increase in the compressive strength was observed as the sintering temperature increases, which was attributable both to viscous flow sintering and to the concomitant development of crystalline species within the amorphous matrix.

Interestingly, fully amorphous 3D structures treated at 600°C revealed a compressive strength value comparable to that of 45S5 glass-ceramic scaffolds produced by the same technique (σ_{max} = 0.3–0.4 MPa) [14].

The increase in compressive strength observed in the temperature range of 600–750 °C followed a highly linear trend with R^2 coefficient equal to 0.9986. However, a drop in mechanical properties was observed at 800 °C as a result of a decrease in structure density. However, even including the samples treated at 800 and 850 °C, the overall strength–T_s relationship still remains linear with R^2 = 0.8393 (Figure 5).

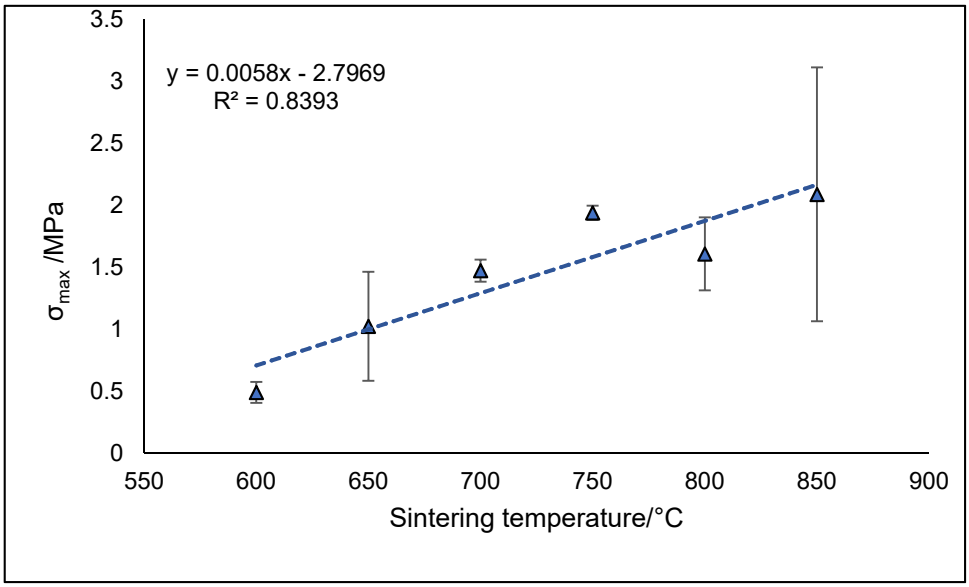

Figure 5. Compressive strength of 47.5B glass and glass-ceramic scaffolds as a function of the sintering treatment.

Despite the higher sintering temperature, it should be noticed that the total porosity ε_0 of scaffolds sintered at 800 °C was remarkably higher with respect to the sample treated at 750 °C, but comparable to that sintered at 700 °C. It is also interesting to underline that, although it was reasonable to assume higher crystallinity levels in scaffolds sintered at 800 °C, the σ_{max} values were comparable in samples with comparable values of ε_0, regardless of crystallinity. This suggests that the porous architecture, compared to the nucleation and growth of crystalline phases, played a predominant role in defining the mechanical performances of the scaffolds under compressive loads.

This hypothesis could be further supported by comparing the 47.5B foam-replicated scaffolds, characterized in the present study, with 47.5B glass-ceramic scaffolds produced by dolomite foaming, as described in a previous work [20]. Specifically, it is interesting to notice how both dolomite-foamed and polymer-replicated scaffolds treated at 800 °C, with ε_0 = 83.0 vol. %, exhibited comparable compressive strength σ_{max} of 1.3 ± 0.4 MPa [20] and 1.6 ± 0.3 MPa, respectively, while the dolomite-foamed scaffolds treated at 850 °C exhibited lower porosity (65.5 ± 7.1 vol. % [20]) and higher compressive strength (3.9 ± 0.9 MPa) with respect to the scaffolds sintered at 850 °C described in the present study.

4. Conclusions

In the present study, the sintering behavior of a bioactive silica-based glass characterized by good sintering behavior and promising bioactive properties was investigated in order to optimize scaffold mechanical properties for bone tissue engineering applications.

Isothermal DTA curves revealed the presence of crystallization exothermic peaks for sintering temperatures above the glass crystallization onset, but diffraction peaks associated to the nucleation of combeite and tremolite crystals were observed also in the samples sintered at 700 °C, indicating a mild beginning of glass devitrification. Material densification upon sintering was found to be comparable in all the samples analyzed, regardless of the temperature used. A decrease in sample density as well as a lower volumetric shrinkage were observed for T_s= 750 and 800 °C as a result of the inhibition in viscous flow caused by the progressive crystallization of the glassy matrix.

All the scaffolds analyzed exhibited mechanical properties comparable to that of human trabecular bone, showing a linear increasing trend as a result of the increase in sintering temperature.

These results suggest that 47.5B-based scaffolds produced by foam replication and sintered at 700°C could represent a good compromise between mechanical performances and bioactive behavior

in body fluids, due to the presence of small crystalline nuclei within a predominant amorphous matrix, improving scaffold strength and ion-exchange processes respectively.

However, it should be noted that all the scaffolds here proposed revealed an attractive potential for bone tissue engineering applications due to the possibility of obtaining highly densified structures able to provide suitable mechanical support to the host tissue while preserving the apatite-forming ability of the material even in a crystallized form.

Author Contributions: Conceptualization, E.F. and F.B.; Methodology, E.F., E.V. and F.B.; Software, E.F. and G.S.; Investigation, E.F., G.S. and F.B.; Resources, C.B., E.V. and F.B.; Data Curation, E.F. and G.S.; Writing-Original Draft Preparation, E.F.; Writing-Review & Editing, G.S., C.B., E.V. and F.B.; Visualization, E.F., G.S. and F.B.; Supervision, C.B., E.V. and F.B. All authors have read and agreed to the published version of the manuscript.

Funding: This research received no external funding.

Conflicts of Interest: The authors declare no conflict of interest relevant to this article.

References

1. Jones, J.R. Review of bioactive glass: From Hench to hybrids. *Acta Biomater.* **2013**, *9*, 4457–4486. [CrossRef]
2. Greenspan, D. Bioglass at 50-A look at Larry Hench's legacy and bioactive materials. *Biomed. Glas.* **2019**, *5*, 178–184. [CrossRef]
3. Hench, L.L. Chronology of Bioactive Glass Development and Clinical Applications. *New J. Glas. Ceram.* **2013**, *3*, 67–73. [CrossRef]
4. Hench, L.L. The story of Bioglass®. *J. Mater. Sci. Mater. Med.* **2006**, *17*, 967–978. [CrossRef] [PubMed]
5. Greenspan, D.C. Bioactive glass: Mechanisms of bone bonding. *Tandläkartidningen Årk.* **1999**, *91*, 1–32.
6. Brauer, D.S. Bioactive Glasses—Structure and Properties. *Angewandte. Chem. Int. Ed.* **2015**, *54*, 4160–4181. [CrossRef] [PubMed]
7. Taha, A.A.; Patel, M.P.; Hill, R.G.; Fleming, P.S. The effect of bioactive glasses on enamel remineralization: A systematic review. *J. Dent.* **2017**, *67*, 9–17. [CrossRef] [PubMed]
8. Sola, A.; Bellucci, D.; Cannillo, V.; Cattini, A. Bioactive glass coatings: A review. *Surf. Eng.* **2011**, *27*, 560–572. [CrossRef]
9. Baino, F.; Verné, E. Glass-based coatings on biomedical implants: A state-of-the-art review. *Biomed. Glas.* **2017**, *3*, 1–17. [CrossRef]
10. Oliver, J.N.; Su, Y.; Lu, X.; Kuo, P.-H.; Du, J.; Zhu, D. Bioactive Materials Bioactive glass coatings on metallic implants for biomedical applications. *Bioact. Mater.* **2020**, *4*, 261–270. [CrossRef]
11. Dorcemus, D.L.; Nukavarapu, S.P. Tissue Engineering of Skeletal Tissues. In *Reference Module in Biomedical Sciences*; Elsevier Inc.: Amsterdam, The Netherlands, 2018. [CrossRef]
12. Sarkar, S.K.; Lee, B.T. Hard tissue regeneration using bone substitutes: An update on innovations in materials. *Korean J. Intern. Med.* **2015**, *30*, 279–293. [CrossRef]
13. Baino, F.; Novajra, G.; Vitale-Brovarone, C. Bioceramics and Scaffolds: A Winning Combination for Tissue Engineering. *Front. Bioeng. Biotechnol.* **2015**, *3*, 1–17. [CrossRef] [PubMed]
14. Chen, Q.Z.; Thompson, I.D.; Boccaccini, A.R. 45S5 Bioglass®-derived glass–ceramic scaffolds for bone tissue engineering. *Biomaterials* **2006**, *27*, 2414–2425. [CrossRef]
15. Wu, C.; Fan, W.; Zhu, Y.; Gelinsky, M.; Chang, J.; Cuniberti, G. Multifunctional magnetic mesoporous bioactive glass scaffolds with a hierarchical pore structure. *Acta Biomater.* **2011**, *7*, 3563–3572. [CrossRef] [PubMed]
16. Fiume, E.; Serino, G.; Bignardi, C.; Verné, E.; Baino, F. Bread-derived bioactive porous scaffolds: An innovative and sustainable approach to bone tissue engineering. *Molecules* **2019**, *24*, 2954. [CrossRef] [PubMed]
17. Cunningham, E.; Dunne, N.J.; Clarke, S.A.; Choi, S.Y. Comparative Characterisation of 3-D Hydroxyapatite Scaffolds Developed Via Replication of Synthetic Polymer Foams and Natural Marine Sponges. *J. Tissue Sci. Eng.* **2011**. [CrossRef]
18. Sepulveda, P.; Jones, J.R.; Hench, L.L. Bioactive Sol—Gel Foams for Tissue Repair Bioactive sol-gel foams for tissue repair. *J. Biomed. Mater. Res.* **2013**, *59*, 340–348. [CrossRef]

19. Jones, J.R.; Hench, L.L. Effect of surfactant concentration and composition on the structure and properties of sol-gel-derived bioactive glass foam scaffolds for tissue engineering. *J. Mater. Sci.* **2003**, *38*, 3783–3790. [CrossRef]
20. Fiume, E.; Tulyaganov, D.; Ubertalli, G.; Verné, E.; Baino, F. Dolomite-Foamed Bioactive Silicate Scaffolds for Bone Tissue Repair. *Materials* **2020**, *13*, 628. [CrossRef]
21. Baino, F.; Barberi, J.; Fiume, E.; Orlygsson, G.; Massera, J.; Verné, E. Robocasting of Bioactive SiO2-P2O5-CaO-MgO-Na2O-K2O Glass Scaffolds. *J. Health Eng.* **2019**, *2019*, 1–12. [CrossRef]
22. Gmeiner, R.; Deisinger, U.; Schönherr, J.; Lechner, B.; Detsch, R.; Boccaccini, A.R.; Stampfl, J. Additive Manufacturing of Bioactive Glasses and Silicate Bioceramics. *J. Ceram. Sci. Tech.* **2015**, *06*, 75–86.
23. Fu, Q.; Saiz, E.; Rahaman, M.N.; Tomsia, A.P. Bioactive glass scaffolds for bone tissue engineering: State of the art and future perspectives. *Mater. Sci. Eng. C* **2011**, *31*, 1245–1256. [CrossRef] [PubMed]
24. Eqtesadi, S.; Motealleh, A.; Pajares, A.; Guiberteau, F.; Miranda, P. Improving mechanical properties of 13–93 bioactive glass robocast scaffold by poly (lactic acid) and poly (ε -caprolactone) melt in fi ltration. *J. Non. Cryst. Solids* **2016**, *432*, 111–119. [CrossRef]
25. Lu, H.H.; El-amin, S.F.; Scott, K.D.; Laurencin, C.T. Three-dimensional, bioactive, biodegradable, polymer-bioactive glass composite scaffolds with improved mechanical properties support collagen synthesis and mineralization of human osteoblast-like cells in vitro. *J. Biomed. Mater. Res. A* **2003**, *64*, 465–474. [CrossRef]
26. Wen, G.; Zheng, X.; Song, L. Effects of P 2 O 5 and sintering temperature on microstructure and mechanical properties of lithium disilicate glass-ceramics. *Acta Mater.* **2007**, *55*, 3583–3591. [CrossRef]
27. Jones, J.R.; Ehrenfried, L.M.; Hench, L.L. Optimizing bioactive glass scaffolds for bone tissue engineering. *Biomaterials* **2006**, *27*, 964–973. [CrossRef]
28. Kaur, G.; Kumar, V.; Baino, F.; Mauro, J.C.; Pickrell, G.; Evans, I.; Bretcanu, O. Mechanical properties of bioactive glasses, ceramics, glass-ceramics and composites: State-of-the-art review and future challenges. *Mater. Sci. Eng. C* **2019**, *104*, 109895. [CrossRef]
29. Tilocca, A. Structural models of bioactive glasses from molecular dynamics simulations. *Proc. R Soc. A* **2009**, *465*, 1003–1027. [CrossRef]
30. Filho, O.P.; Latorre, G.P.; Hench, L.L. Effect of crystallization on apatite-layer formation of bioactive glass 45S5. *J. Biomed. Mater. Res.* **1996**, *30*, 509–514. [CrossRef]
31. Plewinsky, M.; Schickle, K.; Lindner, M.; Kirsten, A.; Weber, M.; Fischer, H. The effect of crystallization of bioactive bioglass 45S5 on apatite formation and degradation. *Dent. Mater.* **2013**, *29*, 1256–1264. [CrossRef]
32. Verné, E.; Bretcanu, O.; Balagna, C.; Bianchi, C.L.; Cannas, M.; Hatti, S.; Vitale-Brovarone, C. Early Stage Reactivity and In Vitro Behavior of Silica-Based Bioactive Glasses and Glass-Ceramics. *J. Mater. Sci. Med.* **2009**, *20*, 75–87. [CrossRef] [PubMed]
33. Fiume, E.; Schiavi, A.; Orlygsson, G.; Bignardi, C.; Verné, E.; Baino, F. Comprehensive assessment of bioactive glass and glass-ceramic scaffold permeability: Experimental measurements by pressure wave drop, modelling and computed tomography-based analysis. *Acta Biomater.* **2020**, in press. [CrossRef] [PubMed]
34. Fiume, E.; Baino, F. Crystallization behavior of SiO 2—P 2 O 5—CaO—MgO—Na 2 O—K 2 O bioactive glass powder. *Biomed. Glas.* **2019**, *5*, 46–52. [CrossRef]
35. Karageorgiou, V.; Kaplan, D. Porosity of 3D biomaterial scaffolds and osteogenesis. *Biomaterials* **2005**, *26*, 5474–5491. [CrossRef]
36. Barberi, J.; Baino, F.; Fiume, E.; Orlygsson, G.; Nommeots-Nomm, A.; Massera, J.; Verné, E. Robocasting of SiO_2-based bioactive glass scaffolds with porosity gradient for bone regeneration and potential load-bearing applications. *Materials* **2019**, *12*, 2691. [CrossRef]
37. Gerhardt, L.-C.; Boccaccini, A.R. Bioactive Glass and Glass-Ceramic Scaffolds for Bone Tissue Engineering. *Materials* **2010**, *3*, 3867–3910. [CrossRef]
38. Barberi, J.; Nommeots-Nomm, A.; Fiume, E.; Verné, E.; Massera, J.; Baino, F. Mechanical characterization of pore-graded bioactive glass scaffolds produced by robocasting. *Biomed. Glas.* **2019**, *5*, 140–147. [CrossRef]
39. Vitale-Brovarone, C.; Baino, F.; Verné, E. High strength bioactive glass-ceramic scaffolds for bone regeneration. *J. Mater. Sci. Mater. Med.* **2009**, *20*, 643–653. [CrossRef]
40. Bretcanu, O.; Chatzistavrou, X.; Paraskevopoulos, K.; Conradt, R.; Thompson, I.; Boccaccini, A.R. Sintering and crystallization of 45S5 Bioglass ®powder. *J. Eur. Ceram. Soc.* **2009**, *29*, 3299–3306. [CrossRef]

41. Huang, R.; Pan, J.; Boccaccini, A.R.; Chen, Q.Z. A two-scale model for simultaneous sintering and crystallization of glass–ceramic scaffolds for tissue engineering. *Acta Biomater.* **2008**, *4*, 1095–1103. [CrossRef]
42. Erasmus, E.P.; Johnson, O.T.; Sigalas, I.; Massera, J. Effects of Sintering Temperature on Crystallization and Fabrication of Porous Bioactive Glass Scaffolds for Bone Regeneration. *Sci. Rep.* **2017**, *7*, 6046. [CrossRef] [PubMed]